 CMC, vol.4, no.1, pp.21-29, 2006

Modelling of Woven Fabrics with the Discrete Element Method

D. Ballhause[1], M. König[1] and B. Kröplin[1]

Abstract: The mechanical behaviour of woven fabrics is dominated by the kinematics of the constituents on the microscopic scale. Their macroscopic response usually shows non-linearities which are due to the mobility of the interlaced yarns. The major deformation mechanisms of fabrics, i.e. the crimp interchange in case of biaxial tension and the trellising motion of the yarns in case of shear, reflect the dependency of the macroscopic material behaviour on the microstructural deformation mechanisms.

We present a novel modelling approach for woven fabrics which is capable to represent directly and locally the microstructure and its kinematics at yarn level. With only a small set of assumptions on the micro-scale the complex macroscopic material behaviour can be directly obtained. The proposed model uses the Discrete Element Method (DEM) for the representation of the fabric's microstructure. It is intrinsically dynamic since the equations of motion are solved numerically for every mass point through an application of an explicit finite difference technique. The model covers the full mobility of the fabric's microstructure while being efficiently enough to model macroscopic patches of the material.

With this model we can study the influence of the different material features of the micro-scale on the macroscopic material behaviour. With some further extensions accounting for coatings or embeddings, the range from pure fabrics to fabric reinforced membranes and composites can be covered. Problems related to large deformations and localization as well as damage can be addressed with the presented modelling approach.

keyword: Woven Fabrics, Textile Membranes, Microstructure Representation, Discrete Element Method.

1 Introduction

Textiles and fabric materials were one of the first mass products of the industrialisation. With the development of more sophisticated fibre materials and the introduction of automated spinning and weaving machinery, also engineering applications of fabric materials gained importance, ranging from tents and sails to more demanding aeronautical applications in balloon and airship skins etc. [Hearle (1985)]. With the development of composite materials another field for the application of fabrics was opened. Fabric materials are seen to be candidates for an automated composite production, because they are easy to handle in dry or pre-impregnated preform and offer a good drapeability, i.e. the capability to form three-dimensional doubly curved shapes [Potluri, Sharma, and Ramgulam (2001)]. Fabric materials show a strongly nonlinear behaviour on the macroscopic scale [Ishikawa and Chou (1983)], which is due to their microstructure of interlaced yarns. Kinematic mechanisms on the yarn-level lead to their typical deformation behaviour. Under biaxial tension, nonlinear stress strain responses occur due to the straightening of one and the increase of waviness of the other yarn family, the so called *crimp interchange*. In the case of shear loading the fabric reacts with a relative rotation of the warp and weft yarns around their crossing points. In pure fabrics this *trellising motion* occurs with only very small resistance. The shear deformation is limited by the effect of *yarn locking* and further shearing usually leads to local buckling of the fabric. All these characteristic effects can still be observed if a fabric is coated or embedded in a deformable matrix material as applied in membrane roofs, airship hulls etc.

Modelling approaches for fabric materials and fabric reinforced membranes have a long tradition. Early experimental investigations and analytical models were reported e.g. from Haas (1917) and Peirce (1937). A common basis for modelling approaches are assumptions on the geometry and kinematic of the unit cell of the fabric, the smallest repeatable unit of the weave geometry. Based on this microstructure approach either analytical relations for the macroscopic material behaviour are derived, see e.g. Kawabata, Niwa, and Kawai (1973a) and Kawabata, Niwa, and Kawai (1973b), or homogenisation methods are applied to obtain macroscopic material

[1] Institute of Statics and Dynamics of Aerospace Structures (ISD), University of Stuttgart, Germany.

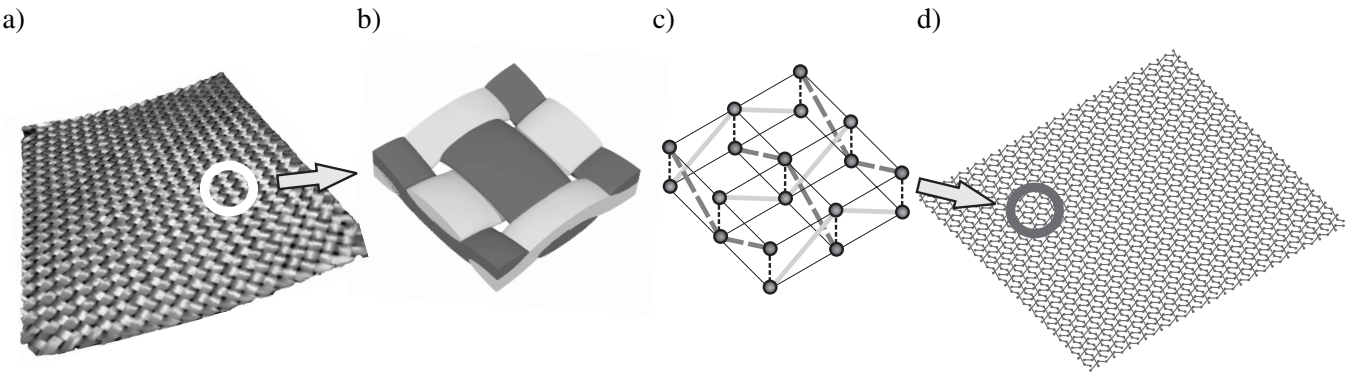

Figure 1 : Discretization of plain weave fabric: a) fabric, b) unit cell, c) model of the unit cell, d) assembled patch.

laws for continuum descriptions like the Finite Element (FE) Analysis, as reported e.g. by Boisse, Borr, Buet, and Cherouat (1997). While the FE approach leads to an efficient tool for design and verification calculations, it often lacks the direct connection between the local microstructure kinematics and the macroscale deformation. Alternatively a direct representation of the microstructure can be chosen. Finite Element simulations of fabric unit cells with small scale meshes on the yarn level, as performed by Glaessgen, Pastore, Griffin, and Birger (1996), usually are restricted to small systems. The incorporation of these micro-scale models on one or more sub-scales into a macroscopic FE analysis leads to the multi-scale models. The models on the different scales are solved successively or in parallel and the information is transported between the related scales as reported e.g. by Kwon and Roach (2004). As an alternative to these continuum based models a discrete modelling approach can be chosen. Based on a simplified representation of the microstructure by an assembly of translatory and rotational springs, a patch of fabric can be simulated preserving the direct connection between macroscopic deformation and the kinematic of the microstructure. Boubaker, Haussy, and Ganghoffer (2002) applied this kind of discrete microstructure representation of fabrics and used energy based minimisation techniques to solve the macroscopic system.

We propose a discrete microstructure model that uses the Discrete Element Method (DEM) (see Bićanić (2004)) and thus applies the numerical solution of the equations of motion of the system. The discrete fabric representation of a plain weave unit cell is depicted in Fig.1, together with the assembled fabric patch. The applied DEM approach is intrinsically dynamic and allows to simulate large displacement and deformation problems, localisation phenomena (e.g. damage evolution) and dynamic loading situations like impact. Furthermore, the microstructure model can be used to explore the complex interactions of fabric materials in critical zones, e.g. seems or joints.

2 Fabric Model

2.1 Discrete Element Method

The presented modelling approach uses the Discrete Element Method. In the framework of this modelling technique a material is represented as a number of discrete mass points m_i as depicted in Fig.2. The mechanical

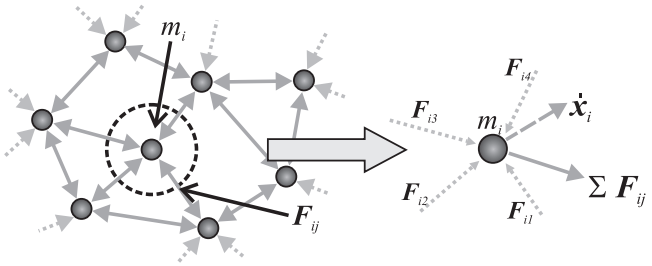

Figure 2 : Discrete representation of material. Interactions of forces on mass points m_i.

properties are introduced by different rheological elements connecting the mass points. The assembly of mass points and rheological elements on the microscopic scale determines the macroscopic material behaviour like Young's Modulus and Poisson's ratio. For each node the state variables position, velocity and acceleration are tracked. The equation of motion for each mass point i reads

$$m_i \ddot{\boldsymbol{x}}_i = \sum^{j} (\boldsymbol{F}_{ij} + \boldsymbol{f}^d_{ij}), \tag{1}$$

with the vector of the acceleration components $\ddot{\boldsymbol{x}}_i$ and the sum of all interaction and damping forces $\boldsymbol{F}_{ij}$ and $\boldsymbol{f}_{ij}^d$ acting between i and its neighbours j. For the numerical integration a Gear predictor-corrector scheme [Allen and Tildesley (1987)] is employed, using time derivatives of the state variables up to the fifth order.

2.2 Fabric Representation

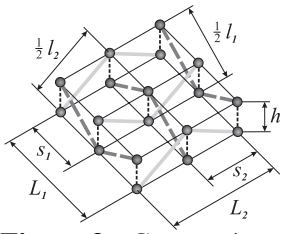

yarn spacing:	s_i
fabric height:	h
length of unit cell	L_i
yarn length in unit cell	l_i

$i = 1,2$ warp and fill direction

Figure 3 : Geometric representation of plain weave fabric: weave parameters.

The presented Discrete Element fabric model is based on a description of the fabric on yarn level, herein referred to as the micro-scale. The discretization of a plain weave fabric unit cell into mass points and interactions and the following assembly of a fabric patch is demonstrated in Fig.1. The mass of the yarns is concentrated into points located on the yarns centerlines at the crossings with the orthogonal yarns. The geometry parameters of the initial state of the DE fabric representation are the yarn spacing of warp and fill s_1^0 and s_2^0 and the fabric height h^0 as depicted in Fig. 3. The fabric height of the model is the distance of the centrelines of the two yarns at the crossings. It can be obtained from the real fabric as half of the sum of the initial transverse yarns thicknesses t_1^0 and t_2^0:

$$h^0 = \frac{t_1^0 + t_2^0}{2}. \tag{2}$$

An important geometric parameter of a fabric is the crimp S_i of warp and fill yarns ($i = 1,2$), which is a measure for the amount of undulation of the yarns in the fabric. It can be defined with the length of the yarn in the unit cell l_i and the length of the unit cell L_i itself as

$$S_i = \frac{l_i - L_i}{L_i} = \frac{\sqrt{s_i^2 + h^2}}{s_i} - 1. \tag{3}$$

The kinematic behaviour of the yarn in the unit cell is described by two interactions: 1) The longitudinal yarn elongation, acting as a linear connection between consecutive mass points of one yarn. 2) The transverse compression between two orthogonal yarns at their crosspoint. The simplifying assumption of piecewise linear yarn members between the crosspoints is a common approach for the description of fabric a unit cell, followed e.g. by Kawabata, Niwa, and Kawai (1973a).

The third interaction type for the fabric unit cell describes the resistance against shear, i.e. the relative rotation of the two yarn families around their crosspoints. In the frame of the present model a relative translatoric movement of the yarns at the crossings is inhibited (pin-joined-model), thus friction effects between the yarns are neglected.

If the influence of a matrix material as an embedding of the fabric should be considered, additional interactions have to be implemented. In the present model additional interactions acting between neighbouring masses of the top and bottom face of the unit cell respectively represent the in-plane tension and shear resistance of the embedding. Fig.4 summarizes all considered interactions for the pure and the coated fabric case.

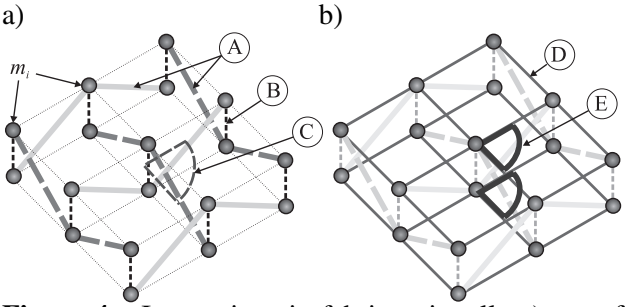

Figure 4 : Interactions in fabric unit cell: a) pure fabric , b) additional matrix interactions. (A) longitudinal yarn, (B) transverse yarn compression, (C) yarn rotation at crossings, (D) matrix elongation, (E) matrix shear.

2.3 Kinematic Interactions

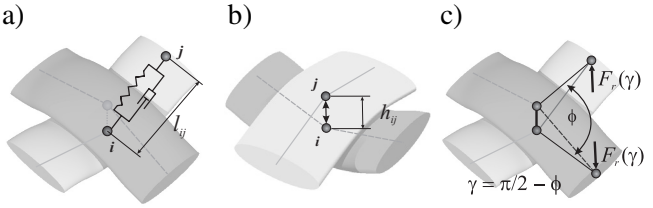

Figure 5 : Fabric interactions: a) longitudinal yarn elongation, b) transverse yarn compression, c) yarn rotation.

The simpliest representation of the longitudinal yarn stiffness is a linear elastic spring element. Due to the dynamic solution technique also dissipative terms should be considered in the system. This can be achieved by applying a Kelvin element, i.e. a spring parallel to a dashpot, as depicted in Fig.5a. In this case the elastic characteristic of the *longitudinal yarn elongation* can be stated as

$$F_{ij}^{l} = k_l \varepsilon_{ij} \quad \text{with} \quad \varepsilon_{ij} = \frac{l_{ij} - l_{ij}^0}{l_{ij}^0}, \tag{4}$$

wherein l_{ij} and l_{ij}^0 are the actual and initial length of the connection line between the two masses i and j and k_l is the linear longitudinal stiffness parameter. The second parameter for the longitudinal yarn elongation is the linear damping coefficient d_l which works on the relative velocity Δv_{ij} between i and j

$$f_{ij}^{d} = d_l \Delta v_{ij}. \tag{5}$$

The *transverse yarn compression* describes the contact between the two yarns at the crossings (Fig.5b). Due to reordering of the fibres in the bundles that form each yarn, the cross section of the yarn can be deformed and the resulting flattening leads to a decrease in the distance of the centerlines of the yarns. This behaviour strongly depends on the type and geometry of the applied fabric. In order to cover a broad range of materials a general exponential form for the contact stiffness is chosen

$$F_{ij}^{c} = k_c {\varepsilon_c}^{n_c} \quad \text{with} \quad \varepsilon_c = \frac{h_{ij}^0 - h_{ij}}{h_{ij}^0}, \tag{6}$$

wherein h_{ij} and h_{ij}^0 are the actual and initial distance of the yarns centerlines. The two parameters for the contact behaviour thus are the contact stiffness k_c and the contact exponent n_c.

The relative *yarn rotation* around the crosspoints as depicted in Fig.5c has to cover two types of phenomena. The first is the usually very small resistance to shear in the range of small rotation angles due to friction and the second is the strongly increasing resistance when the rotation reaches the locking state. The rotational resistance is formulated as a function of the shear angle γ which is related to the intersection angle ϕ of the yarns at the crossing through $\gamma = \pi/2 - \phi$. It has the dimension of a momentum $M^r(\gamma)$ which then is applied as a force F_r on the neighbouring masses. In order to cover the two parts, trellising and locking, it can be described as

$$M_{ij}^{r} = M^t(\gamma_{ij}) + M^L(\gamma_{ij}), \tag{7}$$

with the trellising resistance M^t and the locking resistance M^l. The trellising part is modelled linear elastic as

$$M^t = k_t \gamma_{ij}, \tag{8}$$

with the trellising stiffness parameter k_t. The locking part is implemented similar to the exponential contact law of the transverse yarn compression. The exponential part gives nonzero values when the rotation angle γ reaches the locking threshold γ_L

$$M^L = \begin{cases} 0, & \text{if } \gamma_{ij} < \gamma_L \\ k_L \left(\frac{\gamma_{ij} - \gamma_L}{\gamma_L} \right)^{n_L}, & \text{if } \gamma_{ij} \geq \gamma_L. \end{cases} \tag{9}$$

The locking behaviour is thus controlled by three parameters, the locking threshold γ_L, the locking stiffness coefficient k_L and the locking exponent n_L.

As depicted in Fig.4b the *matrix stretching* is considered in the form of a network of interactions acting between the neighbouring masses at the top and bottom surface respectively. In the basic form of the model these interactions are defined as linear elastic similar to the longitudinal yarn stiffness Eq.4

$$F_{ij}^{m} = k_m \varepsilon_{ij}, \tag{10}$$

with the matrix stiffness parameter k_m.

The shear rigidity of the matrix material, which prevents the relative rotation of the yarns is implemented similar to the trellising interaction in Eq.8 as a linear elastic rotational spring

$$M^s = k_s \gamma_{ij}, \tag{11}$$

with the matrix shear stiffness k_s.

The interactions indicated above complete the basic setup of the DE fabric model. The assumptions for the interactions and their parameters are summarized in Table 1. Extensions of the linear material laws of matrix and yarns in order to describe plasticity or any other non-linear material behaviour can be easily made, since the solution scheme is explicit and the model is implemented in a modular manner.

3 Numerical Results

The application of the DE fabric model is demonstrated by four sample problems, which underline the typical deformation behaviour of fabric materials. In the first two

Table 1 : Summary of interactions and their parameters.

interaction	*type*	*parameter*
longitudinal yarn	yarn stiffness	k_l
	yarn damping	d_l
transverse yarn	contact stiffness	k_c
	contact exponent	n_c
yarn rotation	trellising stiffness	k_t
	locking stiffness	k_L
	locking exponent	n_L
	locking threshold	γ_L
matrix stretching	matrix stiffness	k_m
matrix shear	shear stiffness	k_s

examples the non-linear tensional behaviour is examined. The influence of the transverse compression is studied in a *biaxial tension test*. The *uniaxial tension test* in the second example shows the effects of the crimp interchange and demonstrates the influence of coatings on the tensional behaviour. The shear deformation is the focus of the last two examples. The *bias extension test* of an uncoated fabric patch shows the trellising and shear locking effects, the influence of coatings on the shear deformation is the objective of the simulation of the *picture frame shear test*.

3.1 Biaxial tension

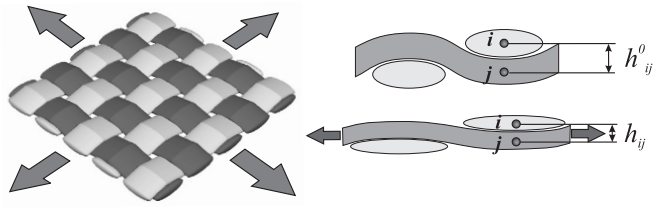

Figure 6 : Simulation of the biaxial tension test with equal forces: effect of transverse yarn compression.

The influence of the transverse yarn compression behaviour can be studied in the case of biaxial tension with equal loads in both directions applied to a symmetric fabric. In this configuration the effects of the crimp interchange are negligible. Fig.6 depicts the simulation of such a test on a small patch of 5×5 yarns for different values of the contact stiffness parameter k_c with fixed contact stiffness exponent $n_c = 4$. A geometry with a ratio of yarn spacing to fabric height of $s^0/h^0 = 10$ is

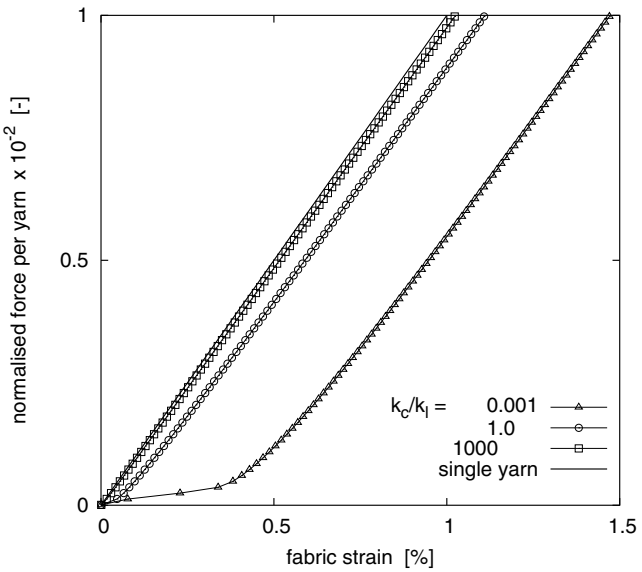

Figure 7 : Simulation results of the biaxial tension test: influence of compression stiffness k_c.

chosen, which results in an initial crimp of $S^0 = 0.5\%$. The simulation results are reported in Fig.7 with the force per yarn normalised by the longitudinal yarn stiffness k_l plotted over the fabric strain. It can be observed that the patch with the stiff contact behaves nearly linear, with a fabric stiffness slightly lower than the longitudinal yarn stiffness itself. Due to the nearly incompressible cross-sections the distance h_{ij} of the crossing yarns is fixed, nearly no compression strain can be observed. In the case of a very soft contact the compressive strain can reach high values, what can be interpreted as a strong flattening of the cross-section of the yarn. The decrease of the crimp results in an offset in the force-strain curve which reaches between 0.3 and 0.4% strain in the given example.

3.2 Uniaxial tension

The geometric non-linearity due to the crimp interchange can be observed, when the biaxial load ratio is unequal. The maximum effect appears in a uniaxial test, where only one direction is loaded while the second direction is left unloaded and unconstrained. A uniaxial test is simulated in order to demonstrate the crimp influence and to illustrate the effect of of the matrix stiffness in case of coated fabrics. Fig.8 depicts the setup and the straightening effect of an applied load. The resulting force over strain plot is shown in Fig.9, again using the normalised

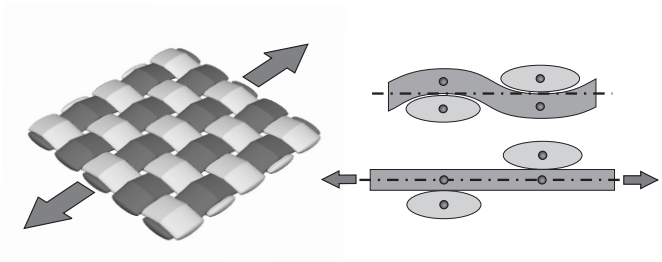

Figure 8 : Simulation of the uniaxial tension test: effect of crimp interchange.

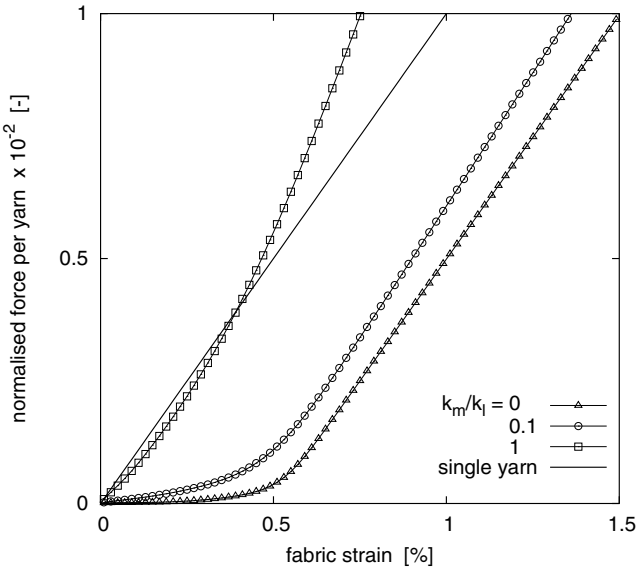

Figure 9 : Simulation results of the uniaxial tension test: influence of matrix stiffness k_m.

yarn force F_y/k_l. The geometry of the patch is the same as in the previous example. Now all parameters are kept constant except the matrix stiffness k_m which is varied from $k_m = 0$, i.e. a pure fabric, to $k_m = k_l$, which represents a very stiff coating. The pure fabric shows an initial range of low resistance, the decrimping zone, in which the loaded yarns are straightened out freely. When the crimp of the yarns is reduced to zero, the fabric is elongated with the stiffness of its single yarns. In the soft coated case the stiffness of the fabric in the decrimping zone is dominated by the matrix stiffness k_m until the stretched state is reached. Then the load is shared between yarn and matrix according to the relation of their stiffnesses.

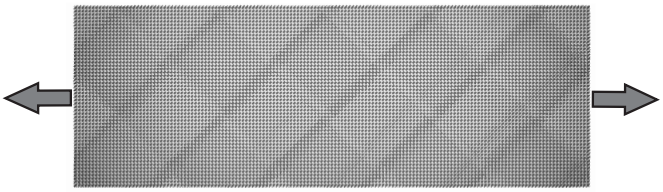

Figure 10 : Simulation of the uniaxial bias extension test on fabric: trellising and locking.

3.3 Bias extension

The shear behaviour of a fabric is studied in the bias extension test. In this setup, a patch of fabric is loaded uniaxially with a bias angle of 45° to the two yarn directions (Fig.10). If a specimen with a length to width ratio greater than one is chosen, no yarn directly connects the two clamps and a centre region of pure shear deformation evolves. For the simulation of the bias extension test a patch with an aspect ration of three is chosen. The fabric geometry is the same as in the previous examples, the locking threshold is set to $\gamma_L = 45°$. Fig.11 shows the total force over elongation of the patch. The two regimes of trellising with low resistance and locking with a steep increase of force can be clearly identified. The deformed state of the simulated patch at 25% strain is given in Fig.12. The left half shows a visualisation of the fabric and the right half the distribution of the shear angle in the fabric's unit cells. In the central shearing zone of the patch, the locking state is reached and some wrinkles appear.

3.4 Picture frame shear test

An alternative setup for the investigation of shearing behaviour of fabrics and membranes is the *picture frame test*. A square patch of material is clamped into a rigid frame. The four side arms of the frame are connected by frictionless joints. If a force is applied on two opposite corners of the frame, a shear deformation is imposed on the material patch, as depicted in Fig.13a. One objective of this kind of test is the determination of the shear angle at which the wrinkling of the material initiates. The setup of a picture frame test of a pure and a coated fabric is simulated on a patch of 60×60 yarns. The boundary conditions of a picture frame are imposed and the resistance force at the corner joints is recorded. The pure fabric is simulated by an activation of the trellising and locking interaction with a locking angle of $\gamma_L = 40°$. The

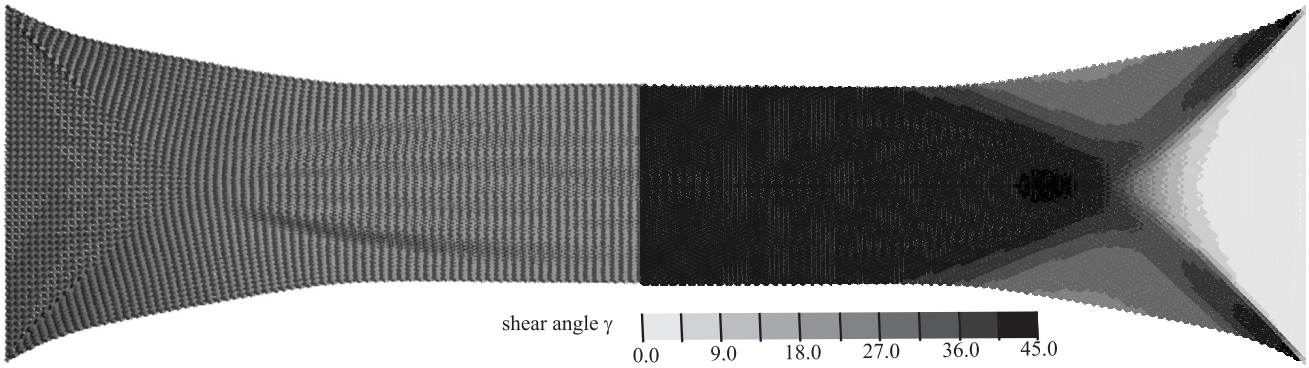

Figure 12 : Simulation results of the uniaxial bias extension test: visualisation of deformed state (left) and distribution of shear angle γ (right) at 25% strain.

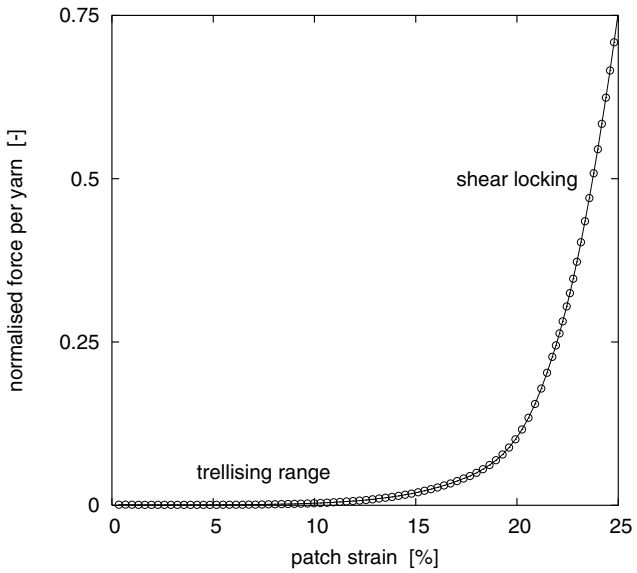

Figure 11 : Simulation results of the uniaxial bias extension test: trellising and locking in force vs. strain plot.

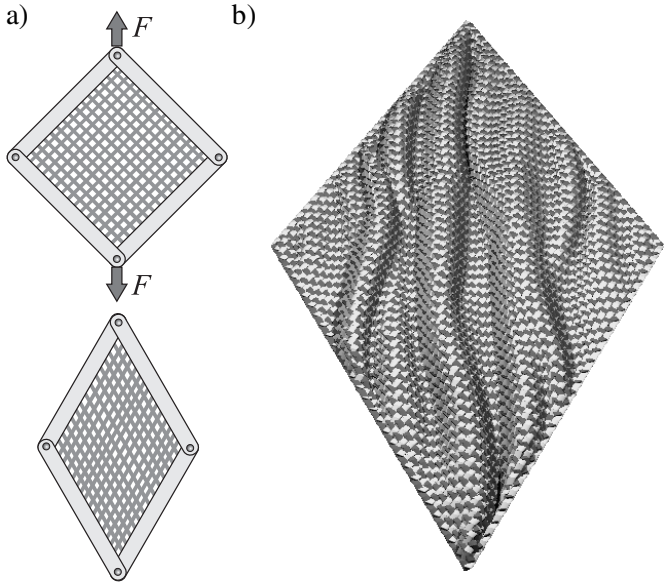

Figure 13 : Simulation of picture frame test: a) shear frame kinematic; b) 3D visualisation of deformed state of coated fabric.

shear stiffness of the coated fabric is set to $k_s = 0.01 k_l s^0$ with the initial yarn spacing of the weave s^0. Fig.13b shows the visualisation of a wrinkled state of the coated fabric at a frame angle of 45°. In Fig.14 the corner force of the frame normalised by the longitudinal yarn stiffness is plotted over the shear angle of the frame for the coated and uncoated fabric. The influence of the coating can be clearly identified: The two distinct ranges of trellising deformation and shear locking of the uncoated fabric vanish when a coating is applied. The influence of the coating on the development of the shear angle in the patch and the initiation of wrinkling can also be observed in the simulation. Fig.15 shows the average local shear angle in the patch over the frame angle for the coated and uncoated fabric respectively. The distribution of the local shear angle of the unit cells of the two materials at frame angles of 30° and 60° is shown in Fig.16. In case of the pure fabric the shear angle follows the frame angle with only small deviation until the locking angle is reached. Upon further shearing of the frame the shear angle in the patch stays nearly constant and wrinkles appear. In the

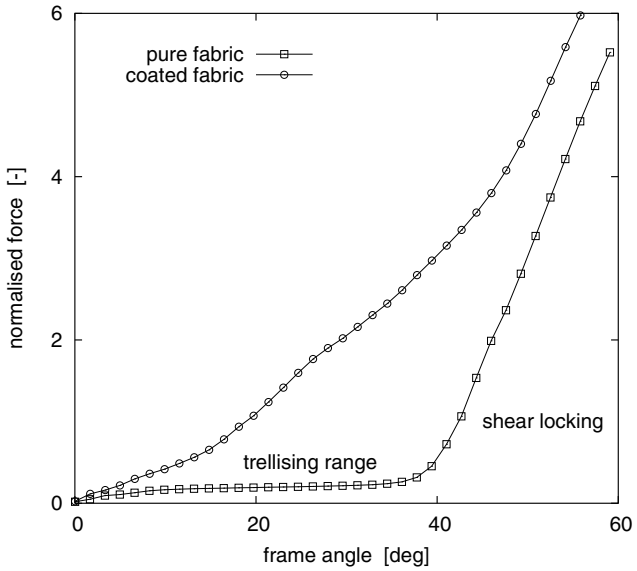

Figure 14 : Simulation results of the picture frame shear test: force vs. frame angle for coated and uncoated fabric.

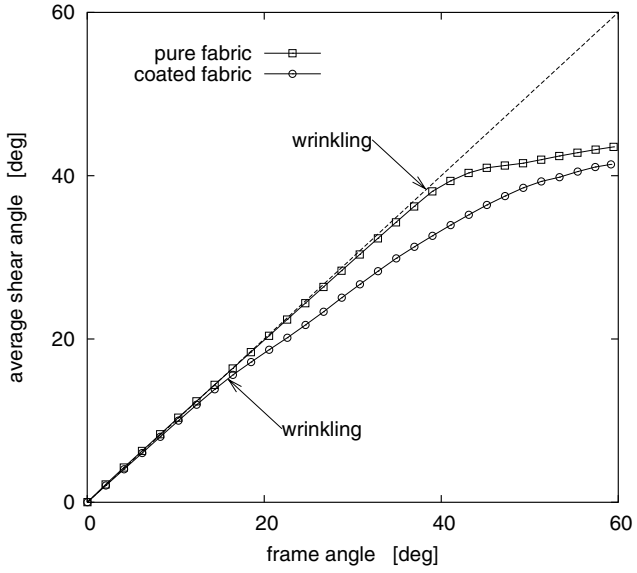

Figure 15 : Simulation results of the picture frame shear test: average shear angle vs. frame angle for coated and uncoated fabric.

case of the coated fabric the wrinkling initiates at much smaller frame angles. The initiation point can be identified in Fig.15 as the point, where the average shear angle of the patch drops below the frame angle, which is in the given example at a frame angle of approximately 16°. The appearing wrinkles can also be observed in the shear

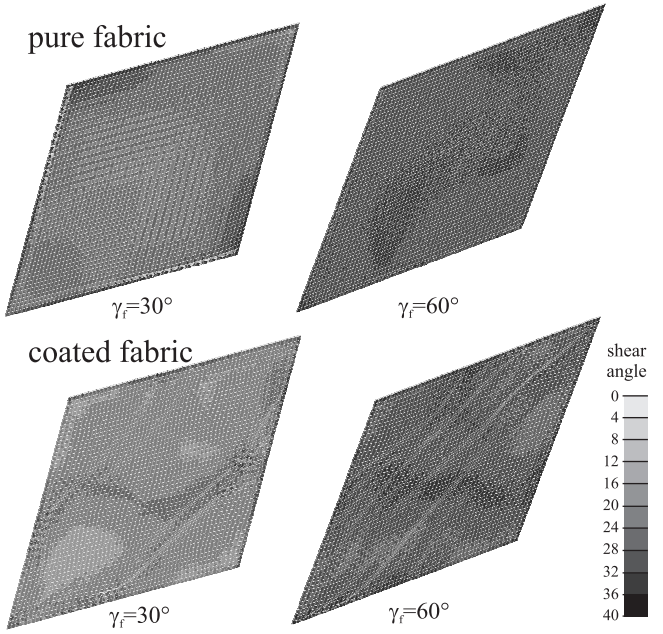

Figure 16 : Simulation results of the picture frame shear test: shear angle distribution in deformed patch of coated and uncoated fabric

angle plots of the coated membrane in Fig.16.

4 Conclusions

We developed a model for fabrics and fabric reinforced materials in the framework of the Discrete Element Method. The complex non-linear deformation behaviour of this class of materials is a consequence of the discrete microstructure formed by interlacing yarns. Within the presented modelling approach this microstructure is modelled directly in an abstracted manner by a small number of interactions. As demonstrated by four application examples the macroscopic response of fabrics can be obtained for uncoated fabrics as well as for coated fabrics or membranes. The application of the numerically efficient solution technique of the DEM enables the simulation of macroscopic patches of fabric materials with a direct representation of the microstructure in the frame of a dynamic solution scheme. With the full information about the local microstructure available throughout the simulation a range of applications could benefit from this approach. Examples are the forming simulation of textile composite preforms, tearing and rupture of fabrics and membranes or the simulation of impact on the fabric.

Acknowledgement: This work was supported by the German Science Foundation (DFG) in the frame of the Research Training Group 285.

References

Allen, M.; Tildesley, D. (1987): *Computer Simulation of Liquids*. Oxford University Press.

Bićanić, N. (2004): Discrete element method. In Stein, E.; de Borst, R.; Hughes, T.(Eds): *Encyclopedia of Computational Mechanics*, volume 1, chapter 11, pp. 311–338. John Wiley & Sons.

Boisse, P.; Borr, M.; Buet, K.; Cherouat, A. (1997): Finite element simulations of textile composite forming including the biaxial fabric behaviour. *Composites Part B*, vol. 28 B, pp. 453–464.

Boubaker, B.; Haussy, B.; Ganghoffer, J.-F. (2002): Modèles discrets de structures tissées: Analyse de stabilité et de drapé. *Comptes Rendus Mecanique*, vol. 330, no. 12, pp. 871–877.

Glaessgen, E. H.; Pastore, C. M.; Griffin, O. H.; Birger, A. (1996): Geometrical and finite element modelling of textile composites. *Composites Part B*, vol. 27, no. 1, pp. 43–50.

Haas, R. (1917): The stretching of the fabric and the deformation of the envelope in nonrigid balloons. *NACA Report*, vol. 16, no. 1, pp. 147–250.

Hearle, J. (1985): The new revolution in textile technology. *Physics in Technology*, vol. 16, pp. 269–281.

Ishikawa, T.; Chou, T. (1983): Nonlinear behaviour of woven fabric composites. *Journal of Composite Materials*, vol. 17, no. 5, pp. 399–413.

Kawabata, S.; Niwa, M.; Kawai, H. (1973a): The finite-deformation theory of plain-weave fabrics; part i: The biaxial-deformation theory. *Journal of the Textile Institute*, vol. 64, no. 2, pp. 21–46.

Kawabata, S.; Niwa, M.; Kawai, H. (1973b): The finite-deformation theory of plain-weave fabrics; part iii: The shear-deformation theory. *Journal of the Textile Institute*, vol. 64, no. 2, pp. 62–85.

Kwon, Y.; Roach, K. (2004): Unit-cell model of 2/2-twill woven fabric composites for multi-scale analysis. *CMES: Computer Modeling in Engineering & Sciences*, vol. 5, no. 1, pp. 63–72.

Peirce, F. (1937): The geometry of cloth structure. *Journal of the Textile Institute Transactions*, vol. 28, pp. T45–T96.

Potluri, P.; Sharma, S.; Ramgulam, R. (2001): Comprehensive drape modelling for moulding 3d textile preforms. *Composites Part A*, vol. 32, pp. 1415–1424.